JTTEE5 8:79-86

Assessment of Damage Accumulation in Thermal Barrier Coatings Using a Fluorescent Dye Infiltration Technique

B. Barber, E. Jordan, M. Gell, and A. Geary

(Submitted 22 April 1998; in revised form 20 December 1998)

Thermal barrier coatings, used extensively on hot section gas turbine engine components, weaken and spall after repeated thermal exposure during normal engine operation. A new technique has been developed, involving the use of vacuum impregnation of the porous ceramic with a mixture of epoxy and fluorescent dye (rhodamine-B) and the ASTM C 633-79 direct pull test, to preserve and reveal incipient damage and accumulated damage prior to spallation in thermal barrier coatings. Excellent definition of damage is provided by the dye in electron beam physical vapor deposited coatings, but the damage is more difficult to distinguish in the highly porous plasma coatings. Image processing is used to quantify the area fraction of debonding. For the electron beam physical vapor deposited yttria-stabilized zirconia coating evaluated, a local area fraction of debonding of up to 20% was observed at 80% of spallation life.

Keywords coating spallation, EB-PVD, fluorescent dye, metallography, plasma spray, thermal barrier coatings

1. Introduction

Thermal barrier coatings (TBCs) are used extensively in gas turbine engines to insulate engine parts from the hot gas stream. Thermal barrier coatings applied to internally cooled, hot section components of the turbine engine improve overall engine efficiency by increasing gas temperature and decreasing the volume of cooling gas, thereby extending component life by reducing substrate metal temperature (Ref 1, 2). The ceramic coating can be effectively applied to complex engine parts using either plasma spray or electron beam physical vapor deposition (EB-PVD) processes.

Plasma sprayed and EB-PVD thermal barrier coatings typically consist of a multilayered structure, shown schematically in Fig. 1. The coating process begins with a superalloy substrate material with good creep and fatigue properties. To provide good bonding of the ceramic coating to the substrate, a metallic bond coat such as a vacuum plasma deposited MCrAlY overlay coating or a platinum aluminide (Pt-Al) diffusion coating is applied. For the plasma spray process, the bond coat surfaces are roughened prior to air plasma spraying of the ceramic to provide good mechanical bonding. The bond coat surfaces are processed to be smooth for EB-PVD coatings to provide better chemical bonding and to grow uniform, parallel ceramic columns during the EB-PVD process. The EB-PVD coating system studied is described in more detail in Ref 3.

The coating life is limited because of its susceptibility to failure by ceramic spallation during thermal cycling of the turbine engine. The differing thermal expansion rates of the ceramic, oxide, and bond coat lead to thermal stresses that are largest in the oxide layer. In the case of flat interfaces, the oxide layer is in compression at room temperature, while for wavy interfaces, tensile stresses arise at some locations in the oxide (Ref 4-7). Thermal stresses also lead to plastic strain in the bond coat (Ref 4-7). These stresses and possible chemical effects such as elemental depletion in the bond coat (Ref 8, 9) and ceramic (Ref 10) lead eventually to coating spallation at the locations shown in Fig. 1.

There is considerable interest in determining damage initiation and progression in TBCs in order to (a) provide quantitative data for input to TBC lifetime prediction models, (b) understand failure mechanisms, and (c) use the understanding to modify TBC materials and processing and thereby improve coating spallation life. Until now, it has been difficult to distinguish between damage produced by thermal cycling and that produced by intentional overload failures.

A new technique is described that is used to locate, identify, and distinguish preexisting voids and cracks from new surfaces created from the direct pull test. This technique eliminates ambiguities and uncertainties encountered when distinguishing between damage produced by thermal cycling and subsequent damage caused by the direct pull test.

The new test method integrates techniques and procedures of different, established experimental methods. It uses a fluorescent dye technique similar to that used to reveal polishing artifacts in metallographic sectioning (Ref 11), a direct pull test conventionally used for determining bond strengths of layered materials, and quantitative computer image analysis.

1.1 Impregnation Technique

Vacuum impregnation of porous TBCs with a mixture of epoxy and fluorescent dye (rhodamine-B) has been established as an effective technique for metallographic preparation of coatings for microstructural examination in cross sections.

B. Barber, E. Jordan, and **M. Gell,** University of Connecticut, Storrs, Connecticut; and **A. Geary,** Metallographic Consulting Services, Meriden, Connecticut.

Examining samples vacuum impregnated with the dyed epoxy allows the investigator to distinguish between damage introduced in service and artifacts introduced in sample preparation.

The effectiveness of this technique is illustrated in Fig. 2, which shows a sectioned view of an EB-PVD coating and a plasma sprayed sample vacuum impregnated with the rhodamine-B dye (ACROS Organics, Pittsburgh, Pennsylvania). The dye is shown to penetrate throughout the porous ceramic to the bond coat interface. In the EB-PVD sample (Fig. 2a) the dye penetrates down the parallel ceramic columns. The large dark void between the arrows results from the ceramic debonding from the substrate and is clearly shown as an artifact introduced during sample preparation because the lower surface is devoid of the red dye. In the plasma sprayed sample, in Fig. 2(b), the voids filled with the fluorescent epoxy are surface connected processing voids present before sectioning and metallographic preparation. For both EB-PVD and plasma sprayed TBCs, the intentionally produced processing defects are shown by the dye to be interconnected from the external surface of the ceramic to the thermally grown oxide (TGO).

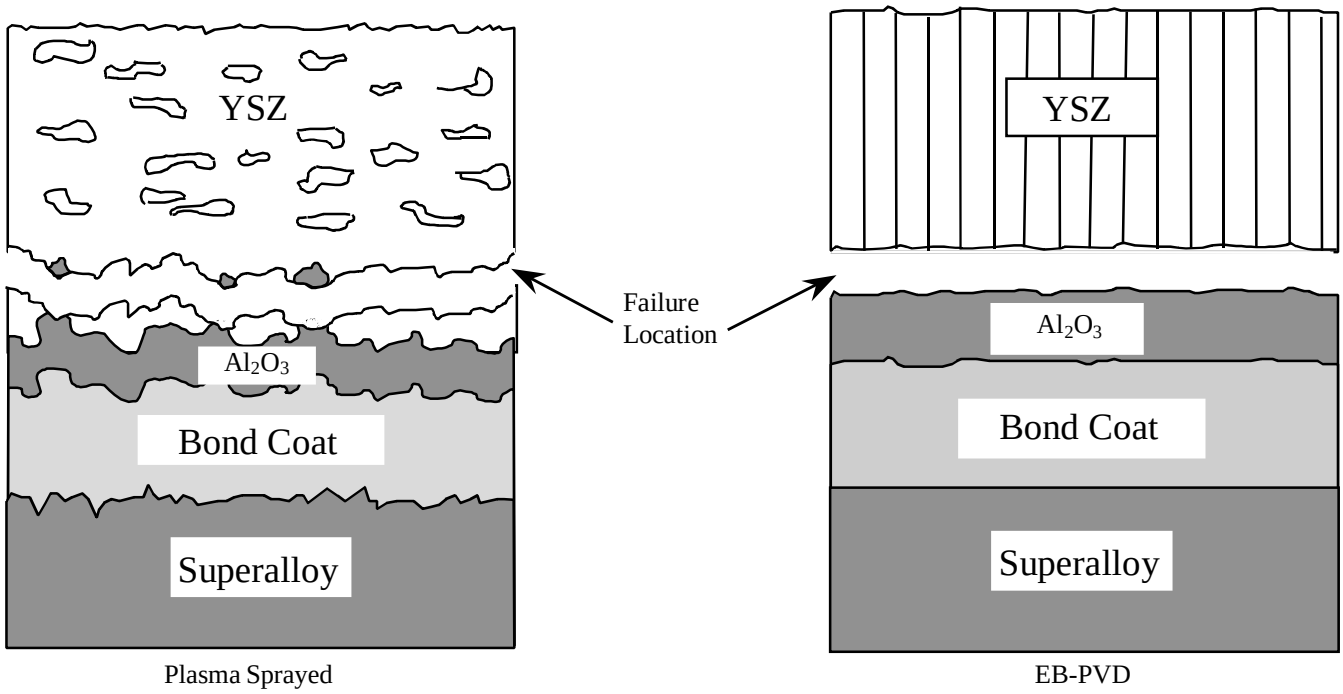

Fig. 1 Schematic of plasma sprayed and Pt-Al / EB-PVD cross sections and failure location

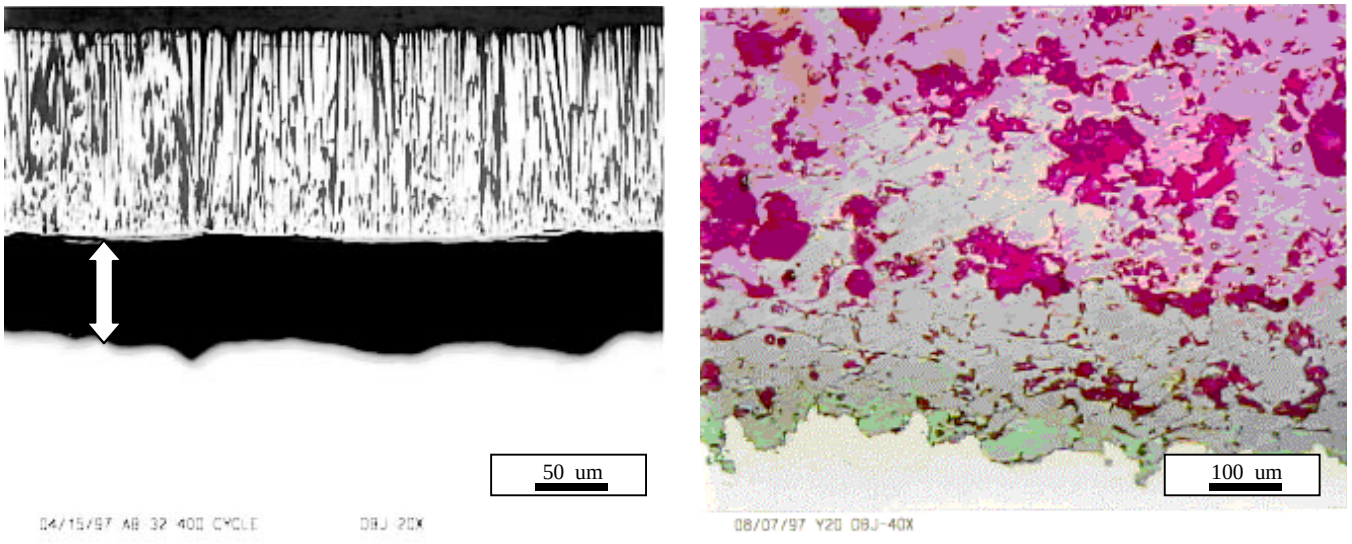

(a) Pt-Al/EB-PVD (b) Plasma Sprayed

Fig. 2 Vacuum impregnated EB-PVD and plasma sprayed sample with rhodamine dye

This dye technique alone is effective when the cross section of the coating is to be investigated. However, it does not provide much information about damage initiation and accumulation occurring in the plane of failure.

The new technique makes it possible for the investigator to make distinctions between cracks, voids, and debonds present at the failure interface from new surfaces created from the direct pull test when the entire fracture surface is investigated. This new method uses vacuum impregnation of a fluorescent epoxy to infiltrate voids, debonds, and cracks developed during thermal cycling beneath the surface of the ceramic. The direct pull test is then implemented to expose the fracture surfaces. Fluorescent markings of the preexisting cracks and voids are left behind after failure for further investigation. Ultraviolet light is used to enhance the visibility of the marking visibility by fluorescing the rhodamine dye for use in area fraction measurement.

2. Experimental Procedure

2.1 Sample Preparation: Pt-Al/EB-PVD and Plasma Sprayed Systems

One EB-PVD and one plasma sprayed coating system were studied. The two coating systems were provided by Advanced Turbine Systems engine developers and coating suppliers using processing identical to that used in commercial turbines. In each case, the coatings were applied to 2.54 cm (1 in.) diameter, 0.3175 cm ($\frac{1}{8}$ in.) thick superalloy disks. Table 1 summarizes descriptions of the coatings and substrate alloys used.

2.2 Thermal Cycling

Some of the coated samples were furnace cycled in air to simulate the thermal exposure seen in the operational heat up and cool down of the turbine engine. In each cycle, the samples were held at 1135 °C (2075 °F) for 60 min and allowed to cool in room temperature air for 10 min. Samples were removed from cyclic tests at various times so the progression of damage in the TBC could be studied.

2.3 Vacuum Impregnation

After thermal cycling, the coated coupons were prepared for vacuum impregnation. The epoxy media used was a two-part Stycast 1269 epoxy (Emerson and Cuming, Inc., Woburn, Massachusetts), which attains a low viscosity during heating to sufficiently penetrate the ceramic coating prior to curing. Three grams of Stycast part A and B were measured and heated separately in an oven at 65 °C (150 °F) for 15 min to reduce their viscosity for improved mixing. After heating, the two parts were thoroughly mixed together with 0.25 g of rhodamine B. The epoxy mixture was poured over the ceramic disk, which was placed ceramic side up in a 3.81 cm (1.5 in.) diameter sample mount.

The mount was then placed in a vacuum furnace. The epoxy temperature was brought to 107 °C (225 °F) while a vacuum of 710 mm Hg was achieved. The sample was maintained at these conditions for 25 min or until the epoxy began to harden. During the impregnation, the vacuum was broken every 3 to 4 min to help the epoxy infiltrate. After vacuum impregnation, the sample was removed from the mount and the excess, unhardened epoxy was dry wiped from the outer surface. The sample was then placed in an oven at 82 °C (180 °F) for an additional 19 h to completely cure the epoxy, which had penetrated beneath the surface of the sample. After curing, the samples either failed using a direct pull test or were sectioned for metallographic evaluation. Figure 3 summarizes the steps for the impregnation process and tensile test.

2.4 Modified ASTM Direct Pull Test

Once the sample was prepared with the fluorescent epoxy, a fracture was introduced using the ASTM C 633-79 "Standard Test Method for Adhesive or Cohesive Strength of Flame-Sprayed Coatings" (Ref 12). The 1 in. diameter test specimen was sandwiched between two 1 in. diameter cylindrical loading fixtures according to the ASTM C 633-79 test method using the high strength epoxy 2214 nonmetallic adhesive (3M Industrial Tape and Specialities Division, St. Paul, Minnesota). The high strength adhesive was found to have a bond strength exceeding 70 MPa (10,150 psi). The loading fixtures were modified to have a 3.81 cm (1.5 in.) length, instead of 2.54 cm (1 in.) as directed by the ASTM C 633-79 standard. The modified loading fixtures produced a more uniform stress state across the test surface (Ref 13) and, therefore, yielded a bond strength more reflective of the intrinsic coating property.

Once the bonding epoxy was cured, the loading fixtures were threaded between two universal joints. The loading system was designed to minimize eccentric bending in the test specimen. An increasing tensile load was applied to the test specimen using a servo hydraulic testing machine. A constant cross head displacement rate of 0.101 cm/min (0.040 in./min) was maintained until failure occurred in the coating. The bond strength was simply determined by dividing the peak load by the area of the failure surface.

The direct pull test induced a failure at the bond coat to ceramic interface for the EB-PVD and a failure just above the bond coat to ceramic interface for the plasma sprayed samples. Of critical importance, the location of the fractures produced by the direct pull test were consistent with those seen in service failures (Ref 14,15).

2.5 Fracture Surface Investigation

Once the ceramic was fractured, the fracture surfaces were observed using both direct optical and optical fluorescent methods. Cracks and voids at this interface were infiltrated with the

Table 1 Description of various layers in TBC coating systems

Superalloy		Bond coat		Ceramic coating	
Alloy designation	**Casting form/alloy type**	**Material**	**Thickness, μm**	**Process**	**Thickness, μm**
N5	Single crystal nickel	Pt-Al	65	EB-PVD	115
MAR-M-509	Polycrystal cobalt	MCrAlY	125	Plasma	300

fluorescent epoxy and were observed using an optical microscope. Fluorescence microscopy was used to enhance the fluorescence and better define the regions impregnated with the fluorescent dye.

3. Experimental Results

3.1 Fracture Surfaces without Rhodamine Dye Infiltration

Electron beam physical vapor deposition specimens were examined to show the damage accumulation in uncycled specimens and in specimens cycled 400 times to approximately 80% of nominal life.

When the fracture surface of the EB-PVD samples was investigated after spallation or after failure in the direct pull test, the mechanism leading to the weakening and failure was not clearly apparent. There was evidence of grain boundary ridges formed during the specimen manufacturing and deep crevices formed in the bond coat during thermal cycling (Ref 3), as seen in Fig. 4. Oxide flakes (see white arrows in Fig. 4) on the metallic bond coat were also apparent across the fracture surface in samples that failed during thermal cycling (Ref 3). When an uncycled specimen was fractured in the direct pull test, ridges at

Mix by weight :
10 parts stycast a
10 parts stycast b
3 parts rhodamine-b

⇓

Pour epoxy mixture over 1" diameter specimen in 1.5" diameter mount

⇓

Impregnate for 25 minutes at 107°C and 710 mm Hg

⇓

Remove sample from mount, wipe off excess epoxy

⇓

Cure 19 more hours at 82° C

⇓

Mount infiltrated specimen between ASTM loading fixtures using EC 2214nm high strength adhesive

⇓

Apply tensile load until coating fails

⇓

Investigate fracture surface

Fig. 3 Summary of dye impregnation process and tensile test

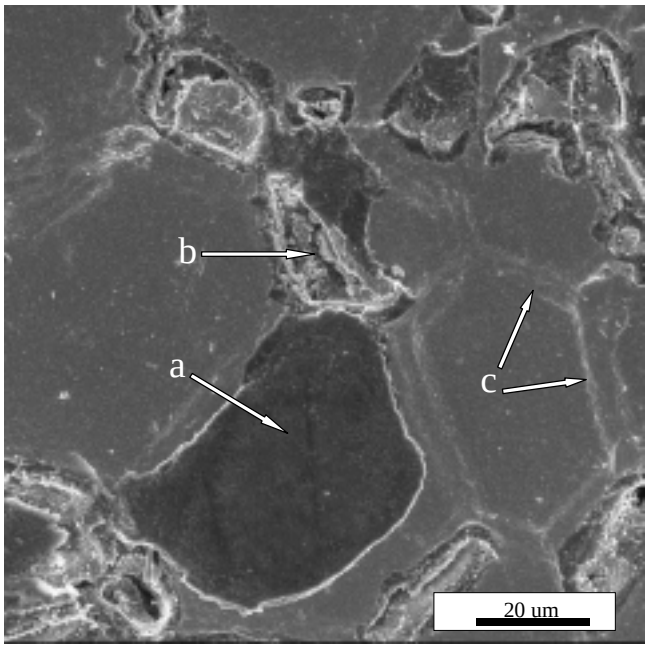

Fig. 4 Fracture surface of spalled Pt-Al / EB-PVD specimen (arrows indicate (a) oxide flake (b) crevice and (c) grain boundary)

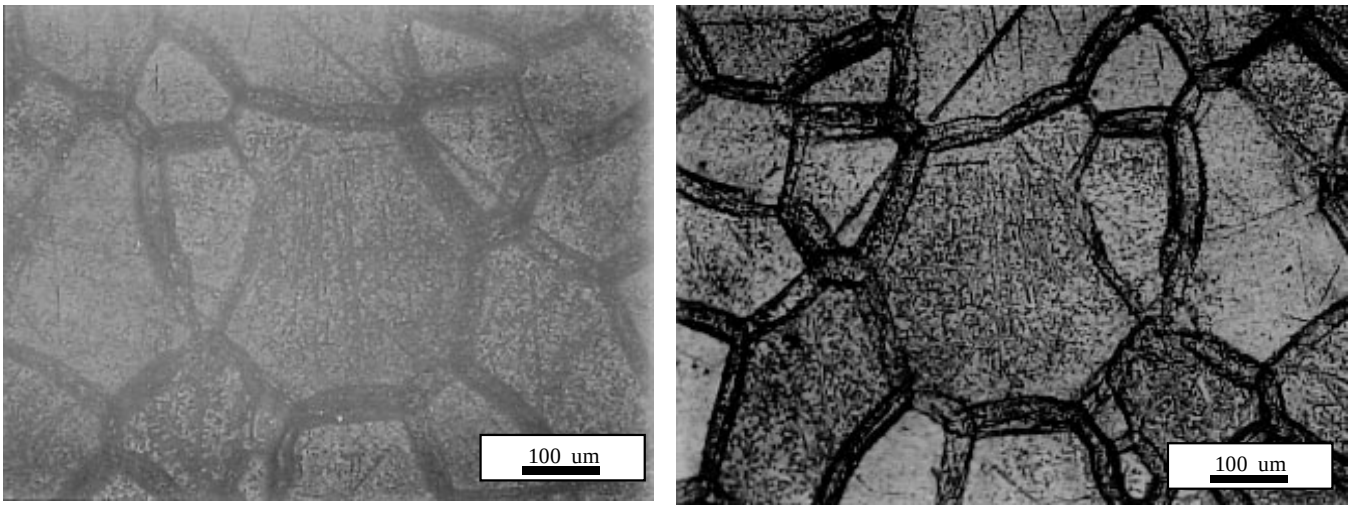

Fig. 5 Paired optical micrograph of 0-cycle Pt-Al / EB-PVD fracture surfaces infiltrated with fluorescent epoxy (ceramic fracture surface (left), opposing substrate fracture (right))

the grain boundaries were evident, however, the thick oxide flakes and deep crevices were not apparent.

Also studied were plasma sprayed samples to show the damage accumulation in zero cycle specimens and in specimens cycled 311 times to approximately 80% of nominal life. In both cases, the failure occurred in the ceramic just above the TGO layer in both the cycled samples and uncycled samples.

3.2 Fracture Surface with Rhodamine Dye Infiltration

The Pt-Al/EB-PVD zero cycle specimen was prepared with the rhodamine dye and fractured in the direct pull test. Figure 5 shows the fracture surfaces at the ceramic to bond coat interface. For both fracture halves, there was no dye evident. This indicated that there were no preexisting flaws such as debonds or voids at the failure interface. The integrity of the zero cycle specimens was consistent with their high bond strengths exceeding 65 MPa (9500 psi) as was measured by the conventional direct pull test without infiltration.

When the same coating system was thermally cycled 400 times and then impregnated with the fluorescent epoxy prior to the direct pull test, regions infiltrated with the fluorescent epoxy became evident on the failure surfaces. Most of these damaged regions corresponded to grain boundaries or grain boundary junctions, as shown in Fig. 6. The damage helps to explain the decrease in bond strength for the EB-PVD to 38 MPa (5500 psi).

The MCrAlY plasma sprayed system was also investigated to correlate the reduction of bond strength in the as-received specimens with thermal cycling. There was dye present in both the cycled and uncycled fracture surfaces. The progression of damage was not as obvious in the plasma sprayed samples. The porous nature and failure location of the ceramic, in both the uncycled and cycled samples, admits excessive dye to the interface, even without damage introduced from thermal cycling. However, there appeared to be more dye present at the failure interface of the cycled specimens when compared to the uncycled sample, suggesting a progression of cracks or debonded regions with thermal exposure.

3.3 Effects of Infiltration on Bond Strengths

There was some question concerning the effect of infiltration on reinforcing the ceramic and hence increasing the apparent bond strengths, as measured by the direct pull test. Preliminary tests on the EB-PVD samples showed that the bond strengths with infiltration fell within the scatter of the bond strengths without infiltration for both the zero cycle and cycled specimens, suggesting the infiltration with Stycast had a minimal effect on the coating integrity. This might be expected because most of the epoxy was prevented from penetrating fully to the failure interface by the thin oxide layer. The effect of infiltration on the bond strength of plasma sprayed samples has not been studied in detail.

3.4 Optical Fluorescence

As shown in Fig. 6, the distinct color of the rhodamine dye helped reveal damage in the TBC microstructure. In some instances, however, the conventional optical microscope did not show a clear distinction between regions infiltrated with the fluorescent dye and regions devoid of the dye. To further enhance the contrast of the dye to the surrounding surfaces, a mercury light source was used in a fluorescence microscope to fluoresce the rhodamine dye. An example of the contrast enhancement is seen in the cycled EB-PVD fracture surface shown in Fig. 7, which compares the same region as seen with and without fluorescence. As clearly shown, all damage is associated with grain boundary regions.

In the plasma sprayed system, the dye was much more abundant in the pores at or near the failure interface than in the EB-PVD system, even without thermal cycling. When the mercury light source was used, the fluorescence was scattered through the semitransparent ceramic, making it more difficult to distinguish between regions with dye from adjacent regions without dye.

3.5 Quantification of Damage Accumulation and Edge Effects

The fluorescence micrographs were then analyzed using MicroGOP 2000/s image analysis software (Contextvision,

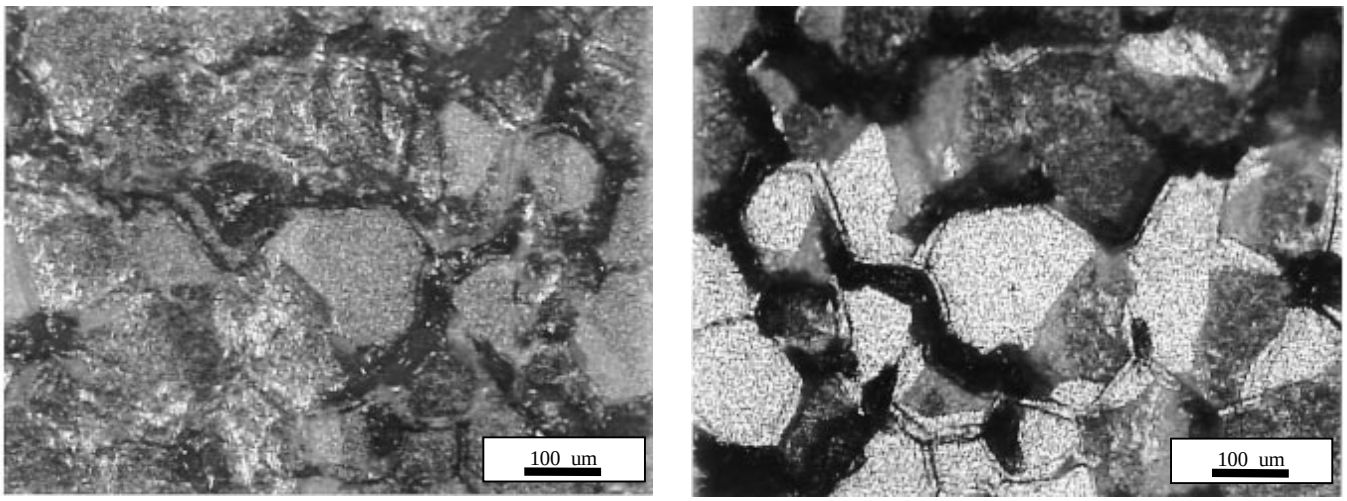

Fig. 6 Paired optical micrographs of cycled Pt-Al / EB-PVD fracture surface infiltrated with fluorescent epoxy (ceramic side left, substrate side right)

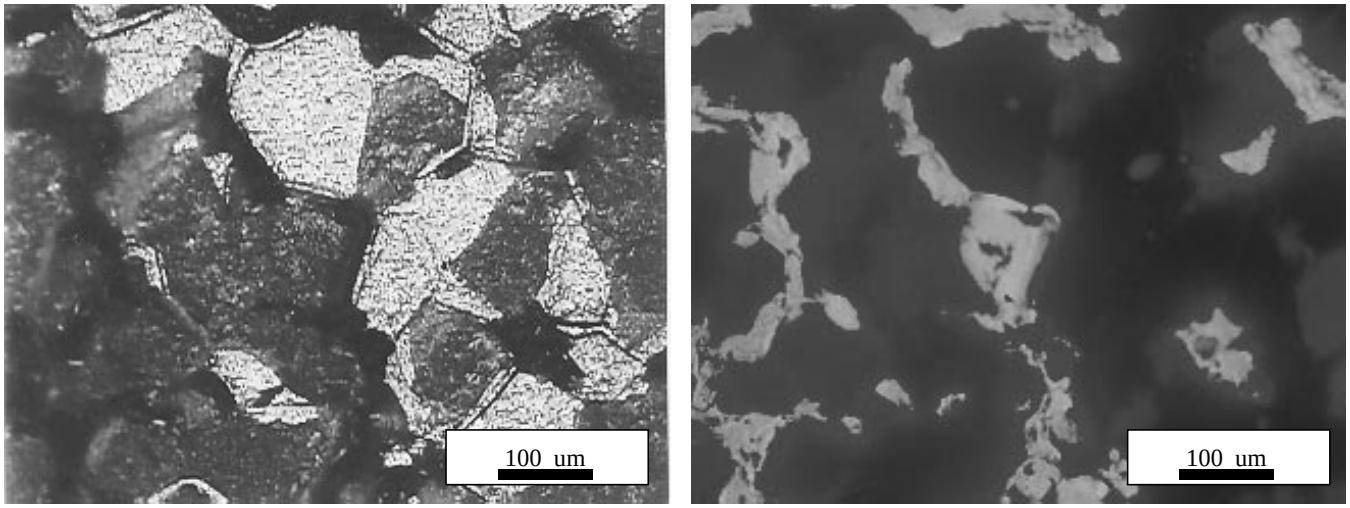

Fig. 7 Optical versus fluorescence micrograph of cycled Pt-Al / EB-PVD fracture surface infiltrated with fluorescent epoxy (conventional optical left, fluorescence right)

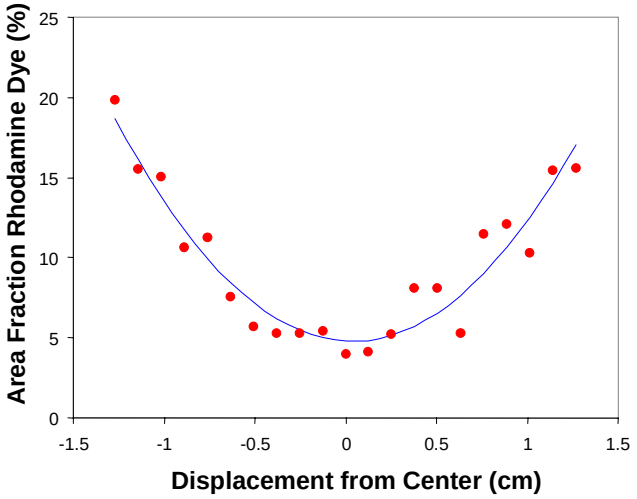

Fig. 8 Variation of area fraction of debonds across the fracture surface of Pt-Al / EB-PVD 400-cycle specimen

Stockholm, Sweden). The software employs a threshholding technique to isolate and quantify the area fraction of the fluorescent dye.

Once a fluorescence micrograph was produced from an area of the sample, image analysis was conducted to determine the area fraction of fluorescence and hence the area fraction of debonds. Figure 8 shows how the area fraction of debonds, as determined by fluorescence micrographs at a magnification of 100×, varied across the 2.54 cm diameter fracture surface of the EB-PVD system.

Area fractions of debonds were found to vary from 4% in the center to 20% near the edge in the 400 cycle specimen. To get an average area fraction of debonding around the entire area of the circular specimen, an area integration must be made from the data plotted in Fig. 8. The data were fit with a parabola that was integrated using the cylindrical shell method and divided by the fracture area of the disk. The average area fraction of debonding as calculated by this method was found to be 11.4%. The increase in damage at the free surface might be correlated with the higher oxide tensile stresses due to edge effects quantified in previously reported finite element analyses (Ref 3). However, the edge effect predicted by this finite element analysis was much more localized than was observed in the rhodamine dye experiment. The magnitude of the scatter in the data can be seen by evaluating the variation in the adjacent data points in Fig. 8 and is approximately ±1%. The error in using this method is difficult to establish because it is not possible to compare the measured result to the actual area fraction of debonding.

3.6 Metallographic Sections

For the EB-PVD system, the rhodamine infiltration in conjunction with the direct pull test focuses attention on the grain boundary ridges where the debonding was observed. To further understand the nature of the debonds and the mechanism of failure, the samples were sectioned to provide another perspective of the damage initiation and accumulation at the grain boundary ridges.

Figure 9 shows a typical coating cross section containing a crevice formed during thermal cycling (Ref 3). The fluorescent epoxy infiltrated into the crevice prior to debonding of the ceramic (see arrows in Fig. 9) due to shrinkage of the mounting epoxy.

The crevice penetrated about 12 μm into the bond coat. A void was apparent within the oxide layer (see single arrows in Fig. 9 and 10), at the ceramic to TGO interface above the crevice. To investigate the nature of the void, serial polishing was employed to show two additional sections through this three- dimensional defect and the associated crevice (see Fig. 10 and 11). Approximately 200 μm (0.008 in.) of material was removed between the sections shown in Fig. 10 and 11 as measured using a micrometer.

These observations suggest that a void initiates to one side of the grain boundary ridge between the ceramic and thermally grown oxide. The void grows until cracking occurs in the protective oxide formed between the ceramic and the bond coat. Once the protective oxide cracked, oxygen was admitted to the bond coat grain boundary, which in turn accelerated oxidation of the bond coat to develop the crevice by forming more

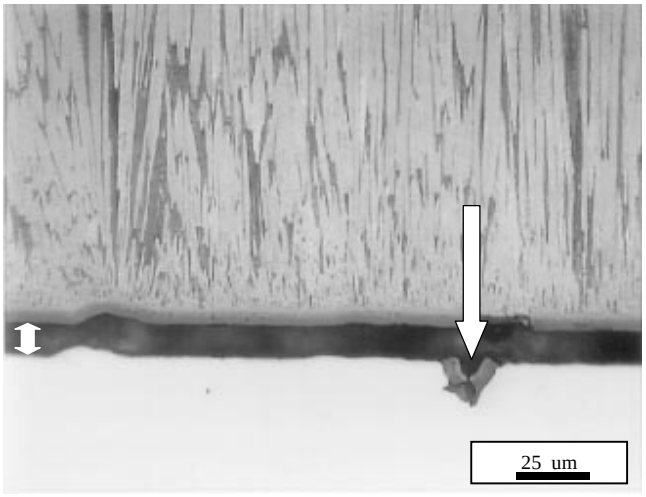

Fig. 9 Cross section of typical crevice in Pt-Al / EB-PVD sample

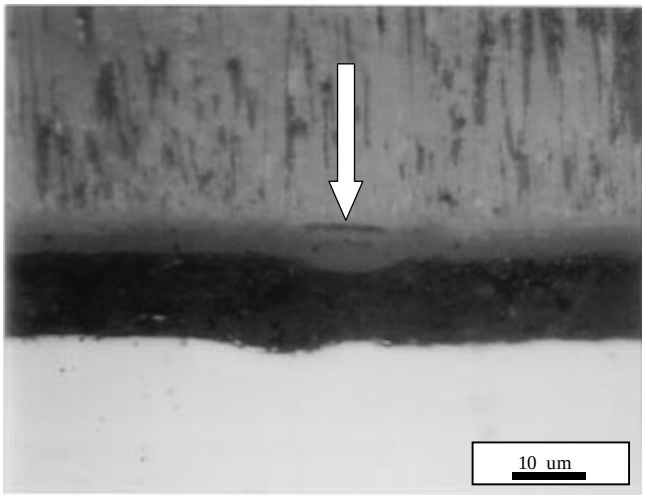

Fig. 10 Cross section of void initiating between the ceramic and substrate in Pt-Al / EB-PVD sample

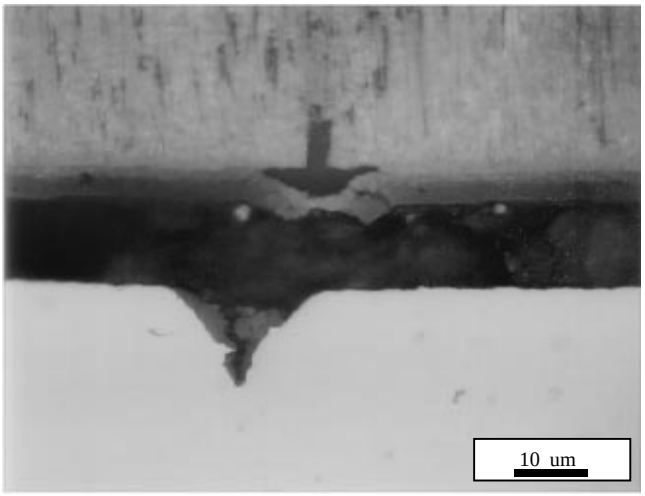

Fig. 11 Cross section of cracks forming around void initiating between the ceramic and substrate in Pt-Al / EB-PVD sample

oxide. These observations have led to a more detailed description of interface debonding, progression, and ultimate spallation (Ref 3).

4. Conclusions

For EB-PVD TBCs, the rhodamine dye infiltration technique in conjunction with the direct pull test provides a useful means for identifying, quantifying, and revealing the nucleation and the progression of cracks, voids, and debonds prior to coating spallation. The area fraction of debonding can be quantified if fluorescence illumination is used in combination with standard quantitative image analysis techniques. These techniques have contributed significantly to determining the failure mechanism in Pt-Al/EB-PVD TBCs. Dye infiltration combined with pull testing has not proven as useful for the plasma sprayed systems due to extensive infiltration of the dye to the failure interface in as-received samples. Cross-section metallographic evaluation and the new infiltration pull test have helped to develop an understanding and identify the failure mechanisms of TBCs. This technique has led to a more detailed understanding of the failure mechanisms in Pt-Al/EB-PVD coatings, as presented by Ref 3.

Acknowledgments

This research was sponsored under subcontract No. 95-01-SR030 from South Carolina Energy Research and Development Center. The authors would like to thank Dr. Daniel Fant, the AGTSR Program Manager, for his continuing guidance and support.

References

1. R.A. Miller and C.E. Lowell, Failure Mechanisms of Thermal Barrier Coatings Exposed to Elevated Temperatures, *Thin Solid Films*, Vol 99, 1982, p 265
2. K.D. Sheffler and D.K. Gupta, "Current Status and Future Trends in Turbine Application of Thermal Barrier Coatings," ASME Paper 88-GT-286, June 1988
3. M. Gell, K. Vaidyanathan, B. Barber, J. Cheng, and E.H. Jordan, Mechanism of Spallation in Pt-Al/EB-PVD Thermal Barrier Coatings, *Metall. Trans.*, Vol 30A, 1999, p 427-435
4. J. Cheng, E.H. Jordan, B. Barber, and M. Gell, Thermal/Residual Stress in Thermal Barrier Coating System, *Acta Mater.*, Vol 46, 1998, p 5839-5850
5. G.C. Chang, W. Phucharoen, and R.A. Miller, Thermal Expansion Mismatch and Bond Coat Oxidation, NASA Conference Publication 2444, 1986, p 357-368
6. J.K. Wright, R.L. William, and R.M. Cammon, Finite Element Analysis of the Effects of Corners on Residual Stress in Protective Oxide Scales, *Mater. Sci. Eng.*, Vol A230, 1997, p 202-212
7. A.G. Evans, M.Y. He, and J.W. Hutchinson, *Acta Metall.*, Vol 45 (No. 9), 1997, p 3542-3554
8. E.P. Busso and F.A. McClintock, Thermal Fatigue Degradation of an Overlay Coating, *Mater. Sci. Eng.*, Vol A161, 1993, p 165-179
9. R.D. Maier, C.M. Scheuermann, and C.W. Andrews, Degradation of a Two-Layer Thermal Barrier Coating under Thermal Cycling, *Am. Ceram. Soc. Bull.*, Vol 60 (No. 5), 1980, p 555-560
10. F. Vasiliu, I. Pencea, V. Manoliu, and I. Dinca, Thermal Stability of Plasma-Sprayed Zirconia Coatings as Related to Substrate Selection, *Am. Ceram. Soc. Bull.*, Vol 64 (No. 9), 1985, p 1268-1271

11. A. Geary, Metallographic Evaluation of Thermal Sprayed Coatings, *Microstructural Sci.*, Vol 19, 1991, p 637-650
12. "Standard Test Method for Adhesive or Cohesive Strength of Flame Sprayed Coatings," C633, *19th Annual Book of ASTM Standards*, Part 17, ASTM, 1979, p 636-642
13. W. Han, E.F. Rybicki, and J.R. Shadley, An Improved Specimen Geometry for ASTM C633-79 to Estimate Bond Strengths of Thermal Barrier Coatings, *J. Therm. Spray Technol.*, Vol 2 (No. 2), 1993, p 145-150
14. S.M. Meier, D.M. Nissley, and K.D. Sheffler, "Thermal Barrier Coating Life Prediction Model Development: Phase II—Final Report," NASA CR-189111, 1991
15. J.T. DeMasi, K.D. Sheffler, and M. Ortiz, "Thermal Barrier Coating Life Prediction Model Development," NASA CR-182230, 1989